PARAMETRIC RESONANCES AND STOCHASTIC LAYER INDUCED BY A PHASE MODULATION*

J.Y. Liu, M. Ball, B. Brabson, J. Budnick, D.D. Caussyn[1], P. Colestock[2], V. Derenchuk
G. East, M. Ellison, D. Friesel, B. Hamilton, W.P. Jones, X. Kang, S.Y. Lee, D. Li
K.Y. Ng[2], A. Pei, A. Riabko, T. Sloan, M. Syphers[3], L. Wang
Indiana University Cyclotron Facility, Bloomington, IN 47408
[1]Physics Department, University of Michigan, Ann Arbor, MI 48109
[2]Fermilab, Box 500, Batavia, IL 60510
[3]Brookhaven National Laboratory, Upton, NY 11973

Abstract

The Hamiltonian system with phase modulation in a higher harmonic rf cavity is experimentally studied on the IUCF cooler ring. The Poincaré maps in the resonant rotating frame are obtained from experimental data and compared with numerical tracking. The formation of the stochastic layer due to the overlap of parametric resonances is discussed. The dependence of the stochastic layer on the voltage of the higher harmonic rf cavity, amplitude and frequency of the phase modulation is studied.

I. INTRODUCTION

The double rf system, *i.e.* a primary rf system plus a secondary rf system working at a higher harmonic, can be used to overcome the space charge effect in low and median energy proton accelerators by reducing the peak current, and provide strong Landau damping against instabilities in high energy accelerators. It has been widely used to enhance the beam intensity in synchrotrons [1].

For particles in a double rf system, the synchrotron equations of motion with respect to the orbiting angle θ are generally given by

$$\begin{aligned} \dot{\phi} &= \nu_s \delta, \\ \dot{\delta} &= -\nu_s (\sin \phi + \epsilon \sin h\phi), \end{aligned} \quad (1)$$

where ϕ is the phase coordinate relative to the primary rf cavity, $\delta = -\frac{h_1 |\eta|}{\nu_s} \frac{\Delta p}{p}$ is the normalized momentum coordinate, and $\frac{\Delta p}{p}$ is the fractional momentum deviation from the synchronous particle, η is the phase slip factor, $\nu_s = \sqrt{\frac{h_1 e V_1 |\eta|}{2\pi \beta^2 E_0}}$ is the synchrotron tune determined by the primary rf system, $h = \frac{h_2}{h_1}$ and $\epsilon = \frac{V_2}{V_1}$ are harmonic and voltage ratios of the primary and the secondary rf cavities.

In previous reports, we have systematically studied the double rf system with $h = 2$ and discussed the stability of particle motion under the influence of parametric resonances by applying external phase and voltage modulations to both rf cavities [2]. We recently studied the controlled beam emittance dilution using the double rf system with higher hamonic ratio by modulating either the primary rf cavity or the secondary one [3]. The controlled beam blow-up is necessary in a high intensity accelerator with a small longitudinal emittance to avoid synchrotron

instabilities and reduce the beam loss during the transition crossing. In this report, we present the study of using the secondary rf cavity with a phase modulation as a perturbation to the primary rf cavity. We analysed parametric resonances and stochastic motions, based on experiment data from the beam experiment CE37F at IUCF. The controlled beam evolution will be discussed in another paper [4].

II. HAMILTONIAN ANALYSIS

With a sinusoidal phase modulation to the secondary rf system, the Hamiltonian can be written as

$$H = \frac{\nu_s}{2} \delta^2 + \nu_s (1 - \cos \phi) + \frac{\nu_s \epsilon}{h} [1 - \cos(h\phi + \phi_m(\theta))], \quad (2)$$

where $\phi_m(\theta) = a_m \sin \nu_m \theta$, a_m and ν_m are amplitude and tune (frequency) of the phase modulation respectively. For a small ϵ/h, we treat the secondary rf system as a perturbation to the primary rf cavity, and therefore we are able to expand the time dependent Hamiltonian in action-angle variables $\{J, \psi\}$ of the unperturbed Hamiltonian [5]. Rewritting the term $\cos(h\phi + \phi_m) = \cos h\phi \cos \phi_m - \sin h\phi \sin \phi_m$, we can expand $\sin h\phi$ and $\cos h\phi$ in the Fourier series,

$$\sin h\phi = \sum_n S_n(J) e^{in\psi}, \quad \cos h\phi = \sum_n C_n(J) e^{in\psi}, \quad (3)$$

where $S_n(J)$ and $C_n(J)$ are *strength functions*, given by the inverse Fourier transform,

$$\begin{aligned} S_n(J) &= \frac{1}{2\pi} \oint \sin[2h \tan^{-1}(\tan \frac{\phi_0}{2} \text{cn}\psi)] e^{-in\psi} d\psi, \\ C_n(J) &= \frac{1}{2\pi} \oint \cos[2h \tan^{-1}(\tan \frac{\phi_0}{2} \text{cn}\psi)] e^{-in\psi} d\psi, \quad (4) \end{aligned}$$

and $\text{cn}\psi$ is the elliptical function. Hence, the term $\cos h\phi$ gives rise only to even harmonics and $\sin h\phi$ to odd harmonics in the first order perturbation. Figure 1 shows the resonance strengths S_1 and C_2 which drive the lowest harmonics of parametric resonances. The small amplitude approximations are compared and found to be good for a range $\phi < 50°$.

In terms of action-angle variables $\{J, \psi\}$, the Hamiltonian of Eq. (2) becomes

$$\mathcal{H} = E(J) + \frac{\nu_s \epsilon}{h} \left[\sum_n \sum_{k=0}^{\infty} S_n(J) J_{2k+1}(a_m) \right]$$
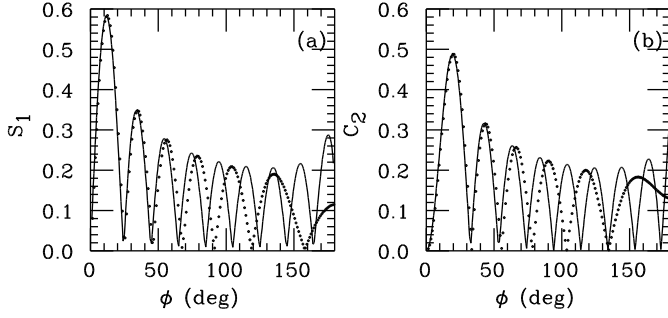
Figure 1. Resonance strengths S_1 and C_2 (solid lines) for strongest parametric resonances, compared with the small amplitude approximations (dotted lines).

$$\times \cos\left(n\psi - (2k+1)\nu_m\theta + \chi_n\right) - \sum_n \sum_{k=1} C_n(J)$$

$$\times J_{2k}(a_m)\cos\left(n\psi - 2k\nu_m\theta + \chi_n\right)\Bigg] \tag{5}$$

where $E(J)$ is the energy of the unperturbed Hamiltonian, and $J_k(a_m)$ is the Bessel function. In Eq. (5), only terms which contribute to parametric resonances are kept. The further analysis of an isolated parametric resonance can be easily accomplished by a canonical transformation. When the modulation tune is near one of the parametric resonances, *i.e.* $k\nu_m \approx n\nu_s$, the perturbation coherently acts on the particle motion.

The parametric resonances are numerically studied in a basis of turn by turn tracking. Figure 2 shows parametric resonances at $\nu_m = 0.6\nu_s$ and $\nu_m = \nu_s$. The overlap of higher harmonic resonances is responsible to the stochasticity near the boundary of the bucket. However, in a dissipative dynamical system such as the IUCF cooler ring, the stochastic motion of particles will not lead a signi®cant beam loss. Instead, particles are damped into the central region of the potential well and form a beam pro-®le with waves on the top. In such a way, the beam emittance is blow-up, depending on the modulation amplitude and frequency. Figure 3 shows the tracking results at $\nu_m/\nu_s = 1$ with a phase damping. The damping rate $\alpha = 15\ s^{-1}$ is used. The ®xed points of resonance islands become attractors as observed in previous experiments [2].
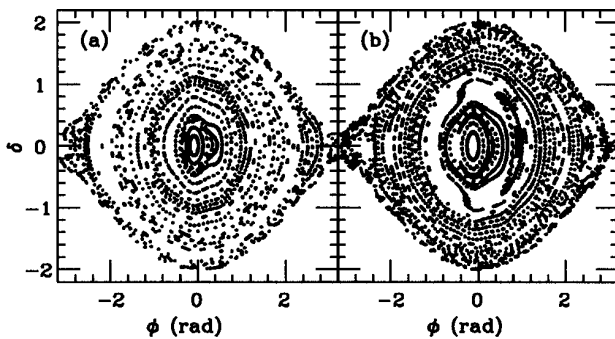

Figure 2. Parametric resonances with $\nu_s = 6.3 \times 10^{-4}$, $\epsilon = 0.2$, $h = 9$ and $a_m = 71°$. In (a), $\nu_m/\nu_s = 0.6$, and in (b), $\nu_m/\nu_s = 1$.
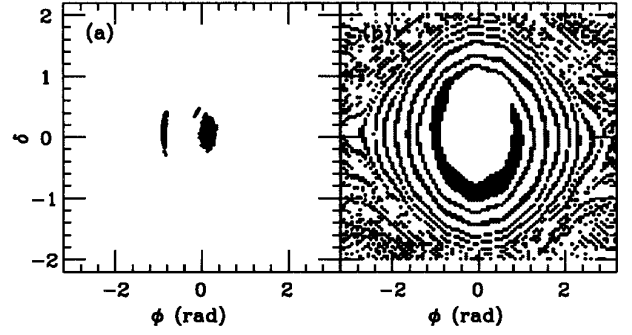

Figure 3. Attractors obtained from tracking 100×100 partcles with $\alpha = 15\ s^{-1}$, $\nu_s = 6.3 \times 10^{-4}$, $\epsilon = 0.2$, $h = 9$, $\nu_m/\nu_s = 1$ and $a_m = 71°$. (a) The ®nal distribution and (b) the initial distribution showing basins of attractors.

III. EXPERIMENTAL MEASUREAMENT

The IUCF cooler ring was operated with a single proton beam bunch at the energy of 45 MeV and the intensity about 100 μA. The cycling time of the proton beam is about 10 seconds with injection and electron cooling being accomplished in about 5 seconds. The electron cooling time is about 300 ms. The beam emittance of the proton beam is electron-cooled to less than 0.3 π mm-mrad in about 3 seconds. The momentum spread $\Delta p/p$ is of order 10^{-4} and the typical bunch length is about $\sigma_l = 10$ ns. The revolution frequency is $f_0 = 1.03168$ MHz. The primary rf cavity and the secondary rf cavity were operated at harmonics $h_1 = 1$ and $h_2 = 9$ respectively. The voltage of the primary rf cavity was set at $V_1 = 285$ v to achieve the synchrtron frequency of $f_s = 650$ Hz (or $\nu_s = 6.3 \times 10^{-4}$), and the secondary rf cavity was varied to obtain a proper voltage ratio to the primary rf cavity.

When the experiment was started, the beam bunch was longitudinally kicked to drive the synchrotron oscillation by phase shifting the control signals for both rf cavities. The phase modulation with controllable amplitude and frequency was added onto the phase shift to the secondary rf cavity. Once the beam is phase kicked, the beam closed orbit x_c was measured from the ratio of the difference (Δ) and sum (Σ) signals of a BPM at a high dispersion location with an accuracy of 0.1 mm. Then the off-momentum variable was calculated from $\Delta p/p = x_c/D_x$, where $D_x \approx 3.9$ m. The Σ signal from this BPM was lead to a phase detector with a range of 720° which generated the phase coordinate by comparing the signal from a pickup loop in the primary rf cavity with a resolution of $0.2°$. A Poincarê map then can be constructed from the digitized $\Delta p/p$ and ϕ data.

Figure 4 shows a set of a typical measured data with $\epsilon = 0.2$, $h = 9$, $a_m = 71°$ and $f_m = 650$ Hz which gave $\nu_m/\nu_s = 1$. In Fig. 4(a) the phase space is plotted each 10 turns for 50000 turns, and in Fig. 4(b) the Poincarêphase map shows a resonance island after data being tranformed to the resonance rotating frame. Because of the weak dissipative damping force of the electron cooling, the motion of the beam centroid is damped into the outer attractor as predicted in Fig. 3. The wiggling of the damping path is due to the time dependent effect. Figure 5 displays the beam pro®les reconstructed from a fast sampling oscilloscope with $\epsilon = 0.2$, $h = 9$, $a_m = 125°$ and $f_m = 600$ Hz, which
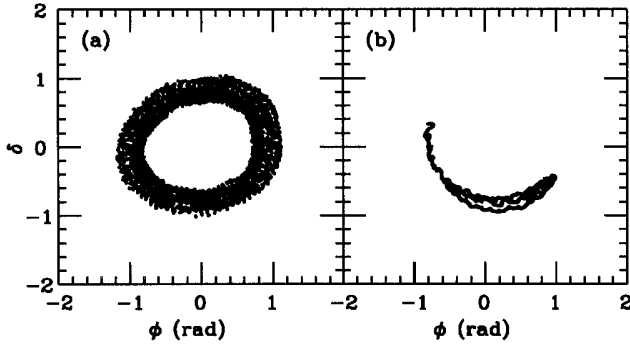
Figure 4. Measured phase space with $\epsilon = 0.2$, $h = 9$, $a_m = 71°$ and $f_m = 650$ Hz ($\nu_m/\nu_s = 1$), (a) original data, and (b) Poincaré phase map after transformation.

shows the evidence of the parametric resonances. Figure 5(a) shows two beamlets obtained about 15 ms after the phase modulation was turned on, and Fig 5(b) shows the final beam profile captured after 25 ms, showing a wave structure resulted from the phase modulation. The beam profiles were extended from a half length of about 10 ns to 50 ns without beam loss.
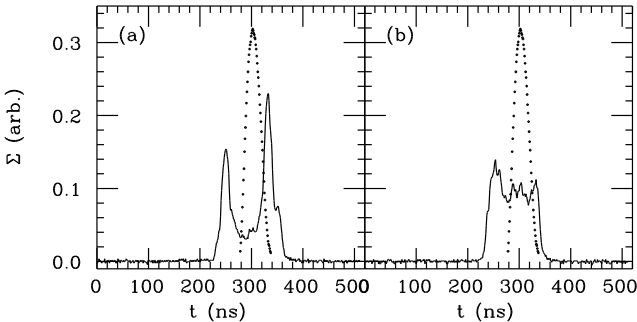

Figure 5. Beam profiles. In (a), two beamlets were due to the first harmonic resonance, and in (b), the beam profile with a wave structure was resulted from the phase modulation. The initial beam profile is plotted as dotted line.

For a given modulation frequency, the stochastic layer exists near the separatrix. As the amplitude of the phase modulation is increased, the stochastic layer increases as well. Numerical simulations indicate that when the beam is kicked inside the stochastic boundary, particle motions in the bunch decohere more rapidly. The change of the damping rates was experimentally observed to depend on the phase modulation. The measurements were done by fixing the phase kicks at $\phi = 60°$, $100°$, $120°$ and $140°$ and varying the modulation amplitude in a step $\Delta a_m = 18°$ for given modulation frequencies $f_m = 600$ Hz, 900 Hz and 1200 Hz. Because the experiment was time-consuming, very coarse steps of the phase kick and the phase modulation were used. Figure 6 shows the measured results of the stochastic boundary versus the modulation amplitude, compared with numerical simulations.

IV. CONCLUSION

In summary, we have studied the parametric resonances due to a phase modulation in the secondary rf cavity. The resonance island was experimentally obtained, which agrees with the theoretical analysis. The beam profiles were evidently related to
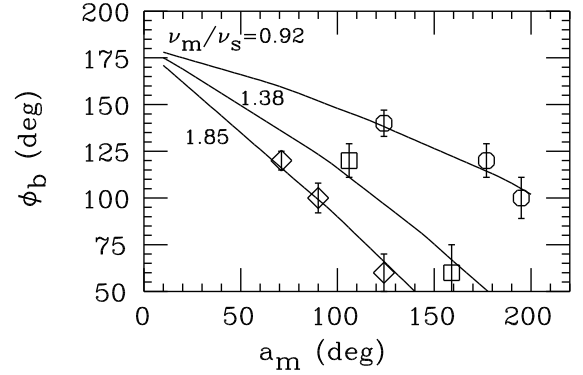

Figure 6. Stochastic boundary as a function of the modulation amplitude for given frequencies (symbols), compared with numerical simulations (solid lines).

the parametric resonances in the beam evolution process. In the measurement of the stochastic layer, we found that this dynamical system was complicated to detect. The diagnostic method of the stochastic layer is expected to work better in a simple system such as the double rf system reported in reference [2].

References

[1] R. Averill et al., Proc. 8th Int. Conf. on High Energy Accelerators, CERN (1971) p.301; P. Bramham et al., IEEE Trans. Nucl. Sci. **NS-24**, 1490 (1977); J.M. Baillod et al., IEEE Trans. Nucl. Sci. **NS-30**, 3499 (1983); G. Gelato et al., Proc. IEEE Part. Acc. Conf., Washington (1987), p.1298.

[2] J.Y. Liu, et al., published on Particle Accelerators; J.Y. Liu, et al., Phys. Rev. E**50**, R3349, (1994)

[3] R. Cappi, R. Garoby and E.N. Shaposhnikova, CERN/PS 92-40 (RF)

[4] L. Wang et al., this procedings.

[5] H. Huang et al., Phys. Rev. E **48**, 4678 (1994); V.V. Balandin, M.B.Dyachkov and E.N. Shaposhnikova, Particle Accelerators, **35** 1 (1991).